Physical Chemistry 2016, 6(1): 11-22
DOI: 10.5923/j.pc.20160601.02

Kinetic and Adsorption Behaviour of Aqueous Cadmium Using a 30 nm Hydroxyapatite Based Powder Synthesized Via a Combined Ultrasound and Microwave Based Technique

Gérrard Eddy Jai Poinern[1,*], Sridevi Brundavanam[1], Suraj Kumar Tripathy[2], Mrutyunjay Suar[3], Derek Fawcett[1]

[1]Murdoch Applied Nanotechnology Research Group, Department of Physics, Energy Studies and Nanotechnology, School of Engineering and Energy, Murdoch University, Murdoch, Western Australia, Australia
[2]Chemical & Bioprocess Engineering Lab, Center of Industrial Technology & School of Biotechnology KIIT University, Campus-11, Bhubaneswar, Odisha, India
[3]School of Biotechnology, KIIT University, Bhubaneswar, Odisha, India

Abstract The removal of heavy metals such as cadmium from contaminated waterways and soils is a very important aspect of environmental remediation. This study investigated the kinetic and adsorption performance of a nanometre scale hydroxyapatite (HAP) synthesised from a combined ultrasound and microwave based technique for the removal of cadmium from an aqueous salt solution. Parameters such as contact time, initial pH, initial cadmium concentration and temperature were investigated. The Freundlich isotherm resulted in a more precise modelling of the communicated experimental data. Maximum monolayer adsorption capacity of absorber was found to be 123.45 mg/g at 298 K. Kinetic studies established cadmium adsorption tended to follow a pseudo-second order model and intra-particle diffusion played a significant role in determining the rate. Adsorption was endothermic, spontaneous and resulted in structural changes to the HAP matrix. The structural changes were investigated using both X-ray diffraction and field emission scanning electron microscopy.

Keywords Nanohydroxyapatite, Adsorption, Cadmium, Ultrasound, Microwaves

1. Introduction

Accumulation of heavy metal contaminants in freshwater supplies, effluents, wastewater, and soils is an extremely important environmental problem that threatens the world. Even in small concentrations, heavy metals are extremely hazardous to living organisms due to their toxicity and tendency to accumulate in the food chain [1, 2]. Therefore, the removal of heavy metals from contaminated water sources is a priority issue in many environmental remediation programs worldwide. Heavy metals such as cadmium (Cd), copper (Cu), chromium (Cr), lead (Pb), mercury (Hg), nickel (Ni), and zinc (Zn) are generally considered the major contaminants of surface water, ground water and soils. The main sources of these contaminants are metal plating industries, mining industries and drainage from abandoned disposal sites. In particular, cadmium is highly toxic, very hazardous for aquatic and soil life and is a known carcinogen in humans [3]. Although cadmium can be found in very small quantities in the natural environment, a significant level of this particular harmful metal is potentially released during industrial and mining processes [4]. Three most common modes of non-ecologically friendly metal uptake by the human metabolic system are via nutritional intake, drinking water and inhalation. Inhalation of cadmium produces significant irritation to the respiratory tract and all three modes of consumption lead to anaemia, osteoporosis, osteomalacia, kidney damage and Itai-itai disease [5-7]. In the case of osseous related diseases, it is the remarkable ion exchange capacity of natural hydroxyapatite (HAP) present in bone tissue that permits the replacement of calcium ions with cadmium ions.

It is due to this extraordinary ability of HAP to accumulate and bind with heavy metals ions such as cadmium within the body, which produces the serious detrimental effect on the health and well-being of an individual. In the case of environmental remediation of contaminated wastewaters, several processes such as filtration, chemical precipitation, electrochemical deposition,

* Corresponding author:
G.Poinern@murdoch.edu.au (Gérrard Eddy Jai Poinern)
Published online at http://journal.sapub.org/pc

ion exchange, adsorption and solvent extraction have all been extensively used with varying degrees of efficiency and cost effectiveness [8-10]. Chemical immobilization by adsorption is one method for reducing the bioavailability of toxic metals via the formation of new stable minerals with lower solubilities in the environment. Several studies have identified the high adsorption capacity of HAP and its ability to combine especially with divalent heavy metals. It is this property that enables HAP to significantly reduce metal ion concentrations in aqueous solutions [11-14]. HAP is a naturally occurring mineral with a hexagonal crystal structure composed of calcium phosphate groups and has the general formula of $[Ca_{10}(OH)_2\ (PO_4)_6]$ for the unit cell. Both chemical and crystallographic studies have also shown that synthetic HAP is similar to the chemical composition of the naturally occurring inorganic component found in teeth and bone tissue [15]. Synthetic forms of HAP have been successfully used in a wide range of applications such as bioceramics for dental and bone repair procedures, absorbents to separate enzymes and proteins during chromatography and as catalysts for dehydrogenation and dehydration of alcohols [16, 17]. The wide range of applications stem from the advantageous surface properties of HAP that include a hydrophilic nature, surface charge, pH, porous structure and 2.6 P-OH surface groups per nm^2 which act as sorption sites [18, 19]. It is the sorption properties of HAP that makes it an attractive absorbent material for potential remediation of heavy metal contaminated water, which adds up from the environment naturally or synthesized and disposed as waste industrial process by-products into the ecosystem.

The synthesis of nanometre scale crystalline HAP (nano HAP) for use as an adsorbent material has been extensively studied and has resulted in techniques such as emulsions, hydrothermal and solution-gelation being used to produce the material [20-22]. However, wet chemical synthesis offers many advantages due to its straightforward and economically efficient protocols during the process. In particular, one advantage is being able to control size and morphology of the forming particles by varying experimental parameters. It is the control of experimental parameters that directly regulates particle nucleation, aging and growth kinetics. Recent studies have also investigated the use of ultrasonic irradiation during wet chemical synthesis to enhance the manufacture of nanometre scale materials [23, 24]. During ultrasonic irradiation, acoustic cavitations create bubbles that grow and then implosively collapse creating localized hot spots with temperatures as great as 5300 K and pressures around 500 atmospheres. The acoustic cavitations also produce very rapid cooling rates that often exceed 1010 K/s [25]. It is the extreme pressures and temperatures experienced during ultrasonic irradiation that promotes the physical effects and chemical reactions which directly influence the size and morphology of the forming particles [26]. Another technique that has been successfully used to improve the synthesis route is microwave heating that significantly reduces reaction times and increases product yields when compared to conventional heating methods [15, 26, 27]. Therefore, incorporating ultrasonic and microwave based techniques into the wet chemical method offers greater efficiency in manufacturing nanometre scale materials. In this study, solutions containing calcium, hydroxyl and phosphate ions were subjected to ultrasound irradiation to form the initial calcium phosphate compounds. This was followed by thermally treating the compounds in a microwave oven to produce the nanometre scale HAP powders used in characterisation and adsorption studies.

The objectives of this study were to first synthesize a nanometre scale HAP powders via a combined ultrasonic and microwave heating based wet chemical method. And secondly, investigate the potential use of the powders as an adsorbent material for the removal of Cd^{2+} cations from aqueous solutions. The synthesized powders were characterized using X-ray diffraction (XRD), field emission scanning electron microscopy (FESEM), energy dispersive spectroscopy (EDS) and Fourier transform infrared spectroscopy (FTIR). The adsorption capacity of the powders was investigated via the removal of Cd^{2+} cations from cadmium contaminated water using a batch equilibrium procedure. Both Langmuir and Freundlich adsorption isotherms were used to model the experimental data. While the kinetic behaviour of the adsorption mechanism were studied using Lagergren's pseudo-first order, McKay & Ho's pseudo-second order and intra-particle diffusion models. Furthermore, the influence of initial Cd^{2+} cation concentration, contact time, temperature, solution pH and thermodynamic parameters were all evaluated from the adsorption measurements.

2. Materials and Methods

2.1. Materials

HAP powders were synthesized from high purity calcium nitrate tetra-hydrate $[Ca(NO_3)_2.4H_2O]$ and potassium di-hydrogen phosphate $[KH_2PO_4]$, while solution pH was controlled by the addition of ammonium hydroxide $[NH_4OH]$. An Ultrasound Processor [UP50H: 50 W, 30 kHz, MS7 Sonotrode (7mm diameter, 80 mm length)] supplied by Hielscher Ultrasound Technology was used to deliver ultrasound irradiation during HAP synthesis. The source of Cd^{2+} ions used in the adsorption studies was high purity cadmium chloride $[CdCl_2]$. All chemicals used in this work were supplied by Chem-Supply (Australia) and all aqueous solutions were made using Milli-Q® water (18.3 MΩ cm^{-1}) produced by an ultrapure water system (Barnstead Ultrapure Water System D11931; Thermo Scientific, Dubuque, IA).

2.2. Synthesis of Nanometres Scale Hydroxyapatite

The synthesis procedure used to produce the nanometre scale HAP powders was developed by the authors and a detailed description is given elsewhere [15, 24, 28]. However, in the interest of completeness a brief description

is presented. The procedure in brief consists of adding a 40 mL solution of 0.32 M calcium nitrate tetra-hydrate into a small glass beaker and then adjusting the solution pH to 9.0 using approximately 2.5 mL of ammonium hydroxide. The solution was then sonicated for 1 h using the Ultrasound Processor set to 50 W and maximum amplitude. During the second hour of ultrasound treatment 60 mL of 0.19 M potassium di-hydrogen phosphate solution was slowly added while the solution pH was maintained at 9.0 and the Calcium/Phosphate [Ca/P] ratio was maintained at 1.67. On completion of the ultrasound treatment, the solution was then subjected to 20 minutes of centrifugation (15,000 g) at room temperature to produce a solid white precipitate. The precipitate was collected, washed and centrifuged for a further 10 minutes. After the second centrifugation, the precipitate was deposited into a fused silica crucible before being placed into a domestic microwave oven for thermal treatment [Set at 100% power for 40 minutes: 1100W at 2450 MHz-LG® Australia]. After thermal treatment, the resultant agglomerated powder was then ball milled until an ultrafine nanometre scale HAP powder was produced.

2.3. Advanced Characterisation Techniques

2.3.1. X-Ray Diffraction (XRD) Spectroscopy

Powder X-ray diffraction (XRD) spectroscopy was used to examine and identify the purity, crystalline size and phases present in synthesized nanometre scale HAP powders. Spectroscopy data was recorded at room temperature, using a Siemens D500 series diffractometer [Cu Kα = 1.5406 Å radiation source] operating at 40 kV and 30 mA. The diffraction patterns were collected over a 2θ range of 20° to 60° with an incremental step size of 0.04° using flat plane geometry with 2 second acquisition time for each scan. The crystalline size of the particles in the powders was calculated using the Debye-Scherrer equation [Equation 1] from the respective spectroscopy patterns.

2.3.2. Field Emission Scanning Electron Microscopy (FESEM)

FESEM was used to study the size, shape and morphological features of the HAP powders before and after the adsorption studies. All micrographs were taken using a high resolution FESEM [Zeiss 1555 VP-FESEM] at 3 kV with a 30 μm aperture operating under a pressure of 1.333×10^{-10} mbar. Samples were mounted on individual substrate holders using carbon adhesive tape before being sputter coated with a 2 nm layer of gold to prevent charge build up using a Cressington 208HR High Resolution Sputter coater.

2.3.3. Energy Dispersive Spectroscopy (EDS)

EDS was used to provide an elemental analysis of the powder samples using an Oxford Instruments energy dispersive system (133 eV resolution), via a 10 mm^2 SATW detector. The analysis was carried out to verify the results of the XRD analysis and to calculate the Ca/P ratio of the synthesised nano-HAP powders.

2.3.4. Fourier Transform Infrared Spectroscopy (FT-IR)

FT-IR spectroscopy of synthesized nanometre scale HAP powders and cadmium loaded HAP powders was carried out using a Perkin–Elmer Frontier FT-IR spectrometer with Universal Single bounce Diamond ATR attachment. Both FT-IR spectra were recorded in the range from 525 to 4000 cm^{-1} in steps of 4 cm^{-1}.

2.4. Batch Adsorption Studies

All adsorption experiments were carried out using the batch equilibrium technique. During experiments the adsorption capacity of absorber for Cd^{2+} ions was investigated. The study also examined the influence of the initial Cd^{2+} ion concentration, contact time, temperature and pH of the test solutions.

The influence of contact time on Cd^{2+} ion adsorption on absorber was examined using aqueous solutions containing 100 mg/L of Cd^{2+} ions (100 ppm) prepared from cadmium chloride [$CdCl_2$]. A sample of 0.1 g HAP taken from the stock solution (1g/L) was added to a 100 ppm Cd^{2+} prepared solution. The magnetic stirring speed was set to 400 rpm, while the temperature of the suspension was maintained at 298 ± 1 K. The pH of the suspension was adjusted by adding drops of 0.1 M NaOH to the suspension and then maintaining the value of 7 throughout the experiment. Sample volumes were taken from the suspension during the mixing process at pre-determined time intervals (10, 20, 30, 40, 60, 90, 120, 180, 240 and 300 min) so that Cd^{2+} ion concentration in the solution could be measured. After each specified time, the sample solution was first filtered using a Whatman® 0.22μm membrane syringe filter and then centrifuged at 15,000 g for 20 minutes. Each time a sample volume was taken, an equal volume was then added to the solution to maintain the initial volume. The concentration of Cd^{2+} ions in the sample solution was determined by inductively coupled plasma atomic emission spectrometer (Varian Vista Axial CCD ICP-AES). All experiments were carried out in triplicate.

The effect of solution pH on adsorption was studied by adjusting the pH from 2 to 12. This was done by treating the solution with either 0.1M HCl or 0.1M NaOH. The temperature was normally set to 298 K, except where temperature variation studies were carried out. After 300 min, the solid was separated from the suspension using a Whatman® 0.22μm membrane syringe filter and the residual cadmium level was measured. The influence of initial Cd^{2+} ion concentration was studied by first preparing a series of Schott reagent bottles containing 100 mL aqueous solutions consisting of varying concentrations of Cd^{2+} ion (50 to 175 mg/L) with an initial pH of 7. Then 1 g/L stock solution containing nanometre scale HAP powder was added (100 mL) into each bottle. The bottles were then sealed and the magnetic stirring speed was set to 400 rpm, while the bottles were thermostatically maintained at the respective isotherm

(283, 293, 303, 313 and 323 K). Measurement of Cd^{2+} concentration levels was carried out at pre-determined time intervals (10, 20, 30, 40, 60, 90, 120, 180, 240 and 300 min). All initial Cd^{2+} ion concentration experiments were carried out in triplicate. The data collected from the adsorption experiments was then used in the subsequent kinetic and adsorption isotherm modelling studies.

3. Results and Discussions

3.1. XRD Spectroscopy Analysis

Analysis of respective powder XRD patterns was used to identify the purity and crystalline size of the synthesised nanometre scale HAP powders used in the adsorption studies. A XRD pattern of a representative pure HAP powder before being used in the adsorption studies is presented in Figure 1. Inspection of the HAP powder (blue pattern in Figure 1) reveals that the reflection pattern matches the known phases present in pure HAP and is consistent with the phases listed in the ICDD database. The pattern also identifies main (h k l) indices found in the HAP sample, namely (002), (211), (300), (202), (310), (222) and (213). The pattern only shows characteristic HAP peaks and there was no evidence of non-HAP phases. In addition, the crystalline size, t (hkl), of each sample was calculated from the respective XRD patterns using the Debye-Scherrer equation [29-31]

$$t_{(hkl)} = \frac{0.9\lambda}{B\cos\theta_{(hkl)}} \quad (1)$$

where, λ is the wavelength of the monochromatic X-ray beam, B is the Full Width at Half Maximum (FWHM) of the peak at the maximum intensity, θ(hkl) is the peak diffraction angle that satisfies Bragg's law for the (h k l) plane and t(hkl) is the crystallite size. The crystallite size calculated from the (002) reflection peak for the sample gave a mean value of 30 nm.

Studies have shown that HAP has a strong selectivity towards divalent metal cations via an ion-exchange mechanism [19, 32]. The results of this study confirm HAPs selectivity towards Cd^{2+} cations and the substitution of Cd^{2+} cations for lattice Ca^{2+} cations. The ion-exchange mechanism was also assisted by the slight difference between the respective ionic radius's of Cd^{2+} (9.7 nm) and Ca^{2+} (9.9 nm).

After each adsorption procedure the solid residue was collected and subjected XRD analysis. Inspection of the XRD pattern for a representative Cd^{2+} loaded sample is presented in Figure 1 and reveals structural changes resulting from Cd^{2+} absorption. The ion-exchange that takes place between the Cd^{2+} and Ca^{2+} cations also results in a very small decrease in the unit cell dimensions and hence volume of the unit cell. Thus, the associated small XRD shifts reported in the literature were also seen in this study and support the ion-exchange mechanism [11, 33]. In this study, the ion-exchange mechanism between Cd^{2+} and Ca^{2+} can be represented by the equivalent molar exchange in general HAP formula Ca_{10-x} Cd_x $(PO_4)_6$ $(OH)_2$, where x can vary from 0 to 10 depending on experimental parameters and reaction time [11].

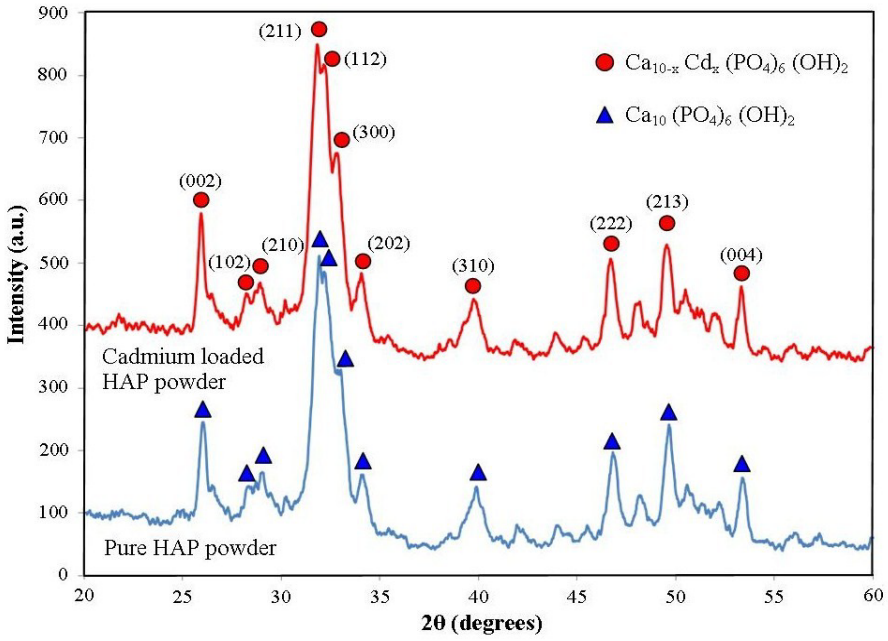

Figure 1. XRD pattern of synthesized nanometre scale HAP powder after milling and drying (Blue), while the second XRD pattern (Red) reflects the maximum uptake of Cd^{2+} of the solid residue at the end of the adsorption study. The study used 1 g/L HAP absorbent, a 100 mg/L Cd^{2+} ion solution, with a pH of 7 and stirred at 400 rpm for a total contact time of 300 min

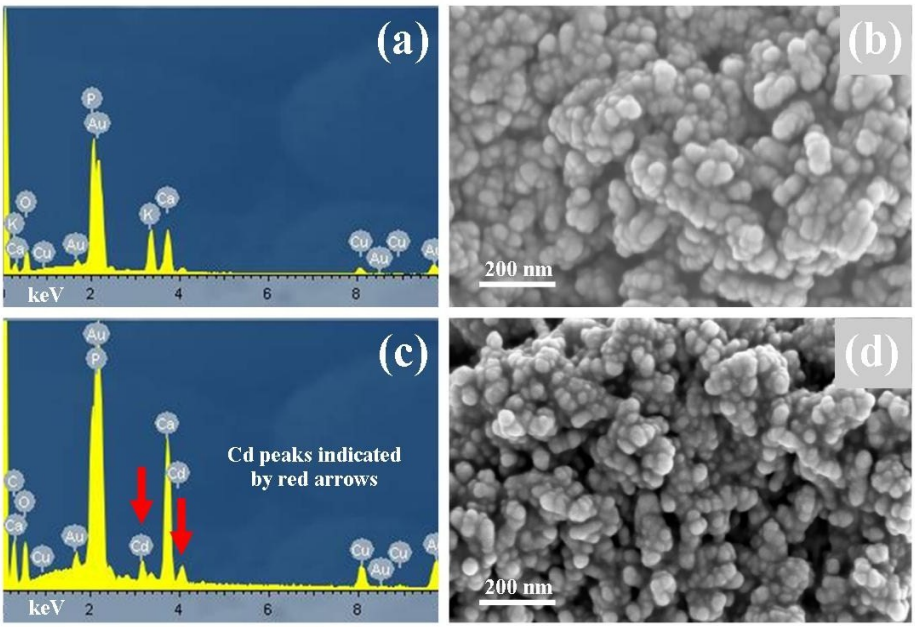

Figure 2. EDS spectrum (a) and FESEM micrograph (b) of unloaded nanometre scale crystalline HAP powder and EDS spectrum (c) and FESEM micrograph (d) of a typical Cd^{2+} loaded HAP residue

3.2. FESEM and EDS Analysis

FESEM was used to study particle size and morphology before and after adsorption studies. A typical micrograph of a pure HAP powder sample is presented in Figure 2(b) and reveals a sphere like particle morphology that is highly agglomerated. The spherical morphology seen is similar to particle morphologies previously reported in the literature [15, 29-31]. Particle size analysis of micrographs revealed a mean particle diameter of 28 ± 5 nm and compared favourably to the XRD determined value of 30 ± 5 nm. After adsorption studies, FESEM analysis was also performed on samples to determine any changes in size or morphology. Figure 2 (d) presents a typical micrograph of the $Ca_{10-x}Cd_x(PO_4)_6(OH)_2$ structure displaying the same agglomerated spherical morphology seen in samples prior to adsorption studies. The mean particle size seen in the Cd^{2+} loaded samples was estimated to be 26 ± 5 nm. The studies have revealed that there was no significant difference in particle size and morphology between unloaded and loaded powder samples. Figure 2 (a) presents a typical EDS spectrum of an unloaded sample showing peaks corresponding to Ca, P, and O, and confirms the chemical composition of HAP. In addition, a number of Au and Cu peaks were also seen in the EDS spectrum. The Au peaks were the product of the Au coating used on the samples, while the Cu peaks are a consequence of X-rays being scattered from the copper grid. Figure 2 (c) presents an EDS spectrum of a representative Cd^{2+} loaded sample and confirms the chemical composition of the sample. The presence of two cadmium peaks (indicated by red arrows) also confirms the results of the XRD analysis discussed above.

3.3. FT-IR Studies

FT-IR spectroscopy and subsequent analysis was used to identify species, functional groups and vibration modes associated with peaks seen in sample spectra taken before and after adsorption studies. Figure 3 presents the results of FT-IR spectroscopy of representative powder samples taken before and after adsorption studies. Starting from the right hand side of Figure 3 with a powder sample prior to adsorption testing. We see three peaks occurring at 561 cm^{-1}, 600 cm^{-1} and 631cm^{-1} that are consistent with ν_4 vibrations normally associated with O-P-O modes. The weaker peak located at 832 cm^{-1} is associated with a carbonate group and clearly indicates the presence of carbonates in the sample. The presence of carbonate ions in the sample is a consequence of atmospheric carbon dioxide interacting with HAP precursors in the synthesis solution and has been reported in the literature by other researchers [34, 35].

The small peak located at 963 cm^{-1} indicates ν_1 symmetric stretching vibrations normally associated with a P-O mode. The strong peak located at 1027 cm^{-1} and the smaller peak located at 1091 cm^{-1} correspond to PO_4^{3-} functional groups. While the weaker peak located at 1374 cm^{-1} corresponds to a CO_3^{2-} functional group. Moving further leftward we encounter a smaller peak located at 1644 cm^{-1} which indicates the presence of a CO_3^{2-} group. The next peak located at 3215 cm^{-1} indicates the presence of absorbed water, while the last identified weak peak located at 3570 cm^{-1} corresponds to OH^- ion vibrations in the HAP crystal lattice. The second pattern presents the FT-IR analysis of a representative powder sample after adsorption testing. The results are very much the same as the pre-adsorption sample, except both 600 and 631cm^{-1} peak intensities are

significantly smaller than those of the pre-adsorption sample as seen in Figure 3 insert. Both peaks are associated with the P–OH groups that act as sorption sites on the surface of the HAP powder [18, 19]. Collectively, their reduced intensities confirm the decrease in the number of free sites available due to Cd^{2+} ion attachment and collaborates the results of XRD analysis.

3.4. Effect of Initial Cd^{2+} Concentration and pH on Adsorption

The influence of initial Cd^{2+} concentration and contact time on adsorption was carried out on initial cadmium concentrations ranging from 50 to 175 mg/L and over contact times ranging from 10 to 300 minutes. Solution temperature was maintained at 298 ± 1 K and solution pH was maintained at 7. During adsorption studies all solutions were magnetically stirred at 400 rpm and concentration measurements were taken at different interval times over a 300 minute test period (10, 20, 30, 40, 60, 90, 120, 180, 240 and 300 min). Figure 4 (a) presents the adsorption results of a HAP absorber (1 g/L) placed in an initial Cd^{2+} ion concentration of 100 mg/L maintained at 298 ± 1 K and stirred at 400 rpm for 300 min. Inspection of Figure 4 (a) reveals maximum Cd^{2+} removal (75 %) occurred after 90 minutes and beyond this period no further adsorption was observed.

The trend was typical of the absorber and further investigations were undertaken to quantify Cd^{2+} ion uptake by increasing initial metal concentrations. The results of these investigations are presented in Figure 4 (b) and reveal increasing initial Cd^{2+} ion concentration (50 to 175 mg/L) tended to produce a corresponding increase in capturing capacity of the absorber (45.75 to 110 mg/g). The increasing trend suggests the higher initial concentrations were able to overcome mass transfer related resistances existing between the aqueous and solid absorber phase by effectively creating a driving force. The effect of pH on adsorption was investigated by repeating batch equilibrium studies using an initial Cd^{2+} ion concentration of 100 mg/L (100 ppm) at various pH values ranging from 2 to 12. Figure 4 (c) presents the results of the pH study and illustrates the effect of pH on adsorption. It is apparent form Figure 4 (c) that Cd^{2+} adsorption steadily increases from pH 2 up to a value of 12 and pH influences the degree of Cd^{2+} removal from the solution. At lower pH values H^+ ions compete with Cd^{2+} ions for binding sites on the absorber surface. However, as the pH increases there is a reduction in competition between H^+, Cd^{2+} and $Cd(OH)^+$ ions and as a result, metal uptake by the absorber increases [11]. The experimental results indicate Cd^{2+} removal was predominantly controlled by adsorption up to a pH of around 8. However, beyond pH 8 Cd^{2+} ion removal was significantly enhanced by cadmium hydroxide precipitation.

3.5. Adsorption Kinetics

Kinetic analysis is essential for understanding any adsorption process. This is because sufficient residence time on the absorber surface is needed to complete the adsorption reaction. The amount of Cd^{2+} ions adsorbed at equilibrium time (q_e) was calculated using equation 2 below:

$$q_e = (C_o - C_e)\frac{V}{m} \quad (2)$$

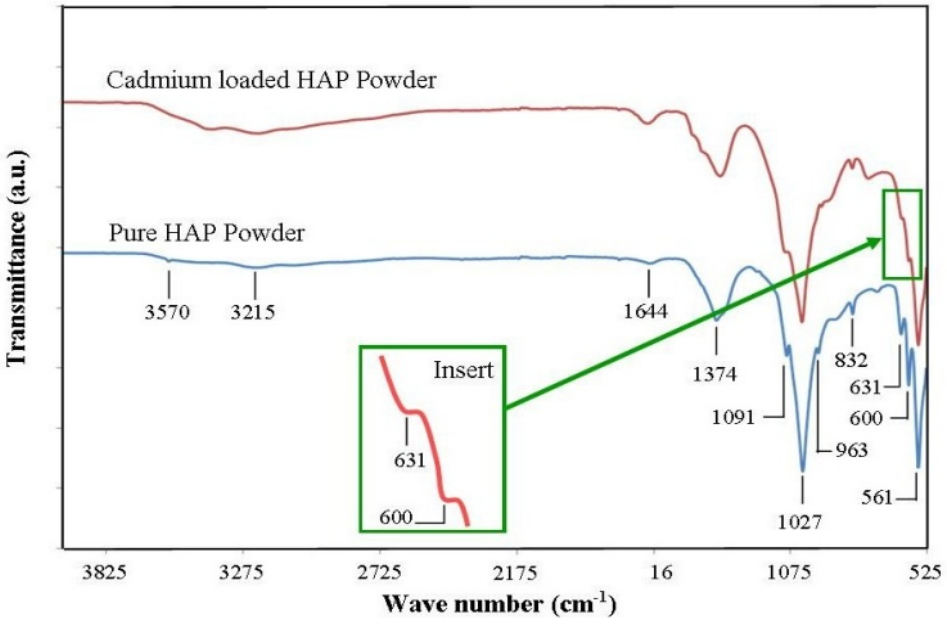

Figure 3. FT-IR Spectroscopy analysis of synthesized pure nanometre scale hydroxyapatite powder after drying and a cadmium loaded HAP residue. The study used 1 g/L HAP absorbent, a 100 mg/L Cd^{2+} ion solution, with a pH of 7 and stirred at 400 rpm for a total contact time of 300 min

where C_o and C_e are the initial and equilibrium concentrations (mg/L) of Cd^{2+} ions in solution, V is solution volume (L) and m is absorber mass (g) used during the experiments. The experimental adsorption data was analysed using three kinetic models: 1) Lagergren's pseudo-first order law; 2) McKay and Ho's pseudo-second-order law, and 3) the intra-particle diffusion model. In the first case, the Lagergren pseudo-first order law [36] is defined by equation 3 below:

$$\log\ (q_e - q_t) = \log q_e - \frac{k_1}{2.303}\ t \qquad (3)$$

where, q_t (mg/g) is adsorption at time t and $k_1(min^{-1})$ is the pseudo-first order adsorption rate constant. In the second case, adsorption kinetics was examined using the McKay and Ho's pseudo-second-order law [37], which is described by equation 4 below:

$$\frac{t}{q_t} = \frac{1}{k_2 q_e^2} + \frac{1}{q_e}\ t \qquad (4)$$

where k_2 (g/min.mg) is the pseudo-second-order rate constant for adsorption. Figure 5 (a) presents kinetic data plotted using the Lagergren pseudo-first order equation (3), while Figure 5 (b) presents kinetic data plotted using the McKay and Ho's pseudo-second-order equation (4). Inspection of the two plots reveals that they are both linear in nature and both models are reasonable representations of the kinetic data. In spite of the reasonable agreement, further analysis reveals that the second order model is superior and has a slightly higher correlation coefficient (R^2) as seen in Table 1.

However, the adsorption process is not a single step event, but instead involves a number of steps. The first step involves diffusion of sorbate from the aqueous solution to the absorber surface. This is followed by the much slower diffusion of sorbate into the internal porous voids of the absorber matrix. Weber and Morris [38] have described this multi-step process using an intra-particle diffusion model which is described by equation (5) below:

$$q_t = k_p\ t^{1/2} + C \qquad (5)$$

where C is the intercept that provides the ideal boundary layer thickness and k_p is the intra-particle diffusion rate constant (mg/g.$min^{1/2}$ g). In the model, the resulting plot of q_t versus $t^{1/2}$ will be linear if the intra-particle diffusion process is involved. In addition, if the linear line passes through the graphs origin, it indicates there is only one rate-controlling step. On the other hand, if the graph is composed of a series of linear plots, then each linear plot will represent a different stage in the adsorption process. The first plot is generally steeper and results from the rapid diffusion of sorbate from solution and its subsequent surface attachment to the absorber. The second linear portion of the graph has a smaller, more gradual gradient and indicates intra-particle diffusion is the prevailing process. In the final equilibrium stage, the gradient levels off and indicates a significant reduction in diffusion due to the low solute concentration. When the adsorption data was plotted using the intra-particle diffusion model a typical multi-gradient line graph pattern was present and is presented in Figure 5 (c). For clarity, only the second and final equilibrium stages are plotted and the modelling parameters such as rate constants, intercepts and correlation coefficients are presented in Table 1.

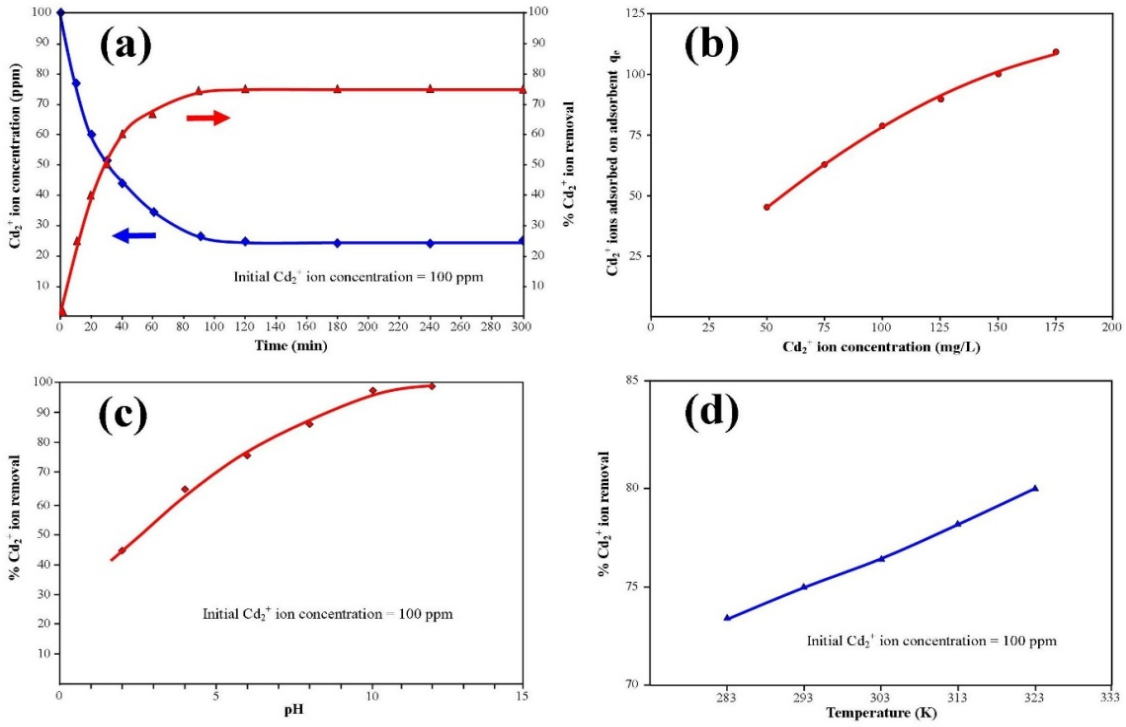

Figure 4. (a) Influence of initial Cd^{2+} concentration and contact time; (b) capturing capacity of the HAP absorbent with increasing initial Cd^{2+} ion concentration (50 to 175 mg/L); (c) the effect of pH on Cd^{2+} adsorption, and (d) the effect of temperature % Cd^{2+} removal

3.6. Adsorption Isotherm

Analysis of the experimental data was important in determining the distribution of Cd^{2+} ions between solution and HAP absorber when the adsorption process had reached its equilibrium state. There are a number of isotherm equations available to model the results of equilibrium data obtained from adsorption systems. The two most widely used equilibrium modelling equations are Freundlich and Langmuir. Freundlich is purely an empirical equation used to fit experimental data. It takes into account surface heterogeneity, the exponential distribution of active adsorption sites and their respective energies over a wide range of concentrations. Langmuir, unlike the Freundlich assumes maximum adsorption occurs when the surface is covered by a monolayer of adsorbate. The equilibrium data for Cd^{2+} ions in solution over a concentration range starting from 50 to 175 mg/L at constant temperature of 298 K, pH of 7, 1 g/L absorbent dose and a contact time of 300 minutes was analysed using Freundlich and Langmuir isotherms. The Freundlich isotherm equation used for modelling the equilibrium data is presented in its linear form below:

$$\log q_e = \log k_F + \frac{1}{n} \log C_e \qquad (6)$$

where k_F and n are Freundlich parameters related to the extent of adsorption and the intensity of adsorption respectively. Both k_F and n parameters were determined via plotting log q_e versus log C_e, the results of which are presented in Figure 6 (a).

Table 1. A comparison between the pseudo kinetic (first and second order) rate constants and intra-particle kinetic diffusion constants and calculated q_e values (pH = 7, initial Cd^{2+} concentration = 100 mg/L, adsorbent dosage = 1 g/L, and agitation rate = 400 rpm)

Pseudo-first-order kinetic model			
Temperature (K)	k_1 (min^{-1})	q_e (mg/g)	R^2
298	0.0317	67.17	0.9964
Pseudo-second-order kinetic model			
Temperature (K)	k_2 (g/mg.min)	q_e (mg/g)	R^2
298	0.00076	80.64	0.9972
Intra-particle kinetic diffusion model			
Temperature (K)	k_p (g/mg.min)	C (mg/g)	R^2
298	7.726	4.448	0.9764

The Langmuir isotherm used for modelling the equilibrium data is expressed mathematically in the linear form by equation (7) below:

$$\frac{C_e}{q_e} = \frac{1}{Q_m b} + \frac{C_e}{Q_m} \qquad (7)$$

where, Q_m (mg/g) is the monolayer adsorption capacity, b (L/g) is the Langmuir constant that is related to the free energy of adsorption, C_e (mg/L) and q_e (mg/g) are the equilibrium concentrations of adsorbate in solution and on the surface of absorber respectively. Using the Langmuir isotherm, a linear plot of equilibrium data was obtained when C_e/q_e was plotted against C_e over the entire Cd^{2+} ion concentration range as seen in Figure 6 (b). The adsorption isotherm is characterized by the two parameters Q_m and b that were determined from the plot. The parameters reflect the surface properties and affinity of the Cd^{2+} ions for the HAP absorber. Both the Freundlich and Langmuir isotherm plots displayed good linear fits and were able to provide intercept and slope parameters which are listed in Table 2.

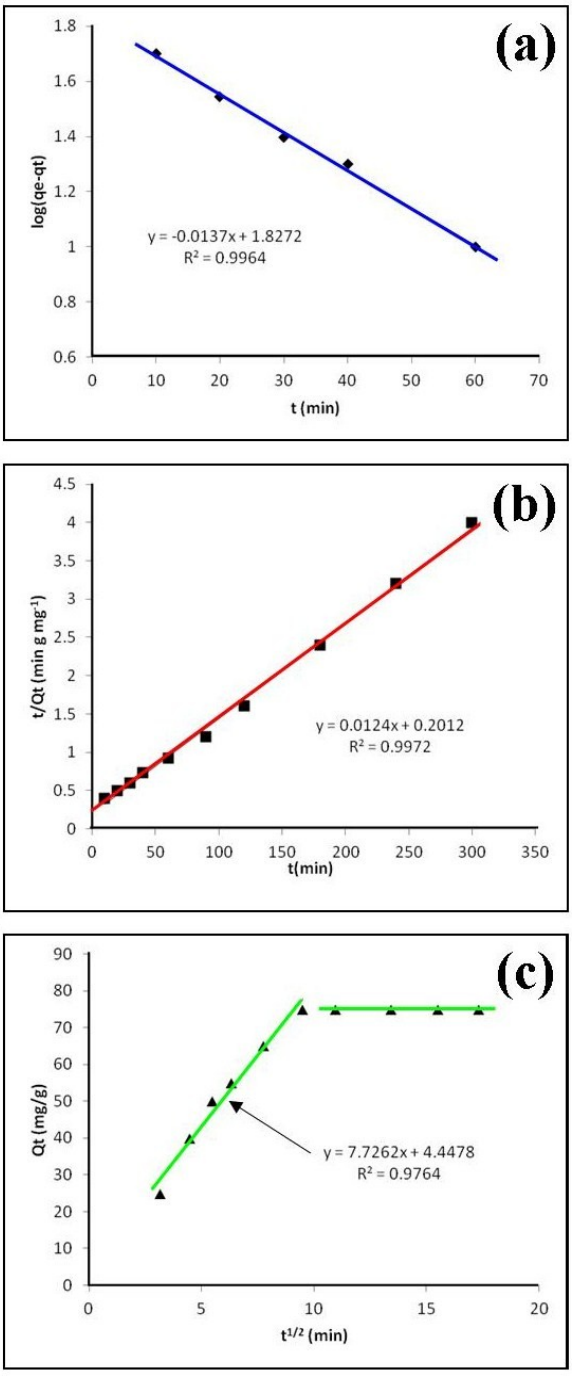

Figure 5. Adsorption data modelled using three kinetic models: (a) Lagergren's pseudo-first order law; (b) McKay and Ho's pseudo-second-order law, and (c) the intra-particle diffusion model. [The study used 1 g/L HAP absorbent, a 100 mg/L Cd^{2+} ion solution, with a pH of 7 and stirred at 400 rpm for a total contact time of 300 min]

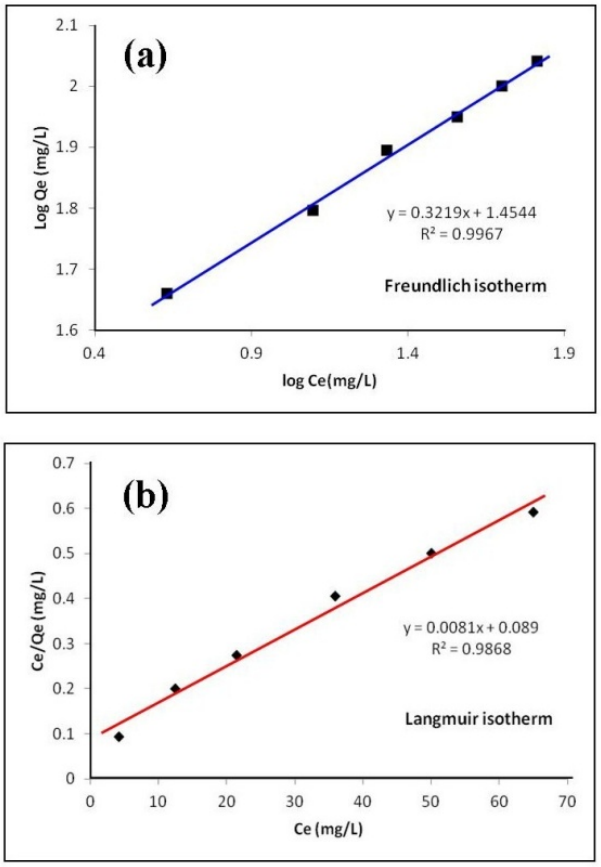

Figure 6. Linear fits of experimental data using (a) Freundlich and (b) Langmuir isotherms [The study used 1 g/L HAP absorbent, a 100 mg/L Cd^{2+} ion solution, with a pH of 7 and stirred at 400 rpm for a total contact time of 300 min]

Table 2. Comparisons between Freundlich and Langmuir adsorption isotherm constants for Cd^{2+} onto nanometre scale hydroxyapatite at 298 K

Freundlich adsorption isotherm constants			
Temperature (K)	k_f (mg/g)	N	R^2
298	28.47	3.106	0.9967
Langmuir adsorption isotherm constants			
Temperature (K)	Q_{max} (mg/g)	b (L/mg)	R^2
298	123.45	0.091	0.9868

For the Freundlich isotherm a value of 3.106 was obtained for n, which fell within the range of 1 to 10 and indicated adsorption was favourable. Furthermore, based on the coefficient of correlation (R^2) values, the Freundlich isotherm provided the best fit of the experimental data. However, unlike Langmuir, the Freundlich isotherm does not predict any maximum occupancy of Cd^{2+} ions on the HAP absorber surface. Instead, it mathematically predicts infinite surface occupancy and the possibility of multi-layered adsorption. Nonetheless, the maximum monolayer adsorption capacity (Q_m) calculated from the Langmuir equation was found to be 123.45 mg/g. Analysis of isotherm data indicates adsorption capacity was the result of increasing equilibrium cadmium concentrations in solution. The increased concentrations were able to increase the numbers of Cd^{2+} ions at the absorber surface and enhance the probability of adsorption.

Table 3. Comparison between cadmium absorption capacities of various materials

Absorbent	**q_m (mg/g)**	**Reference**
Rice husk	2.00	[40]
Olive cake	65.40	[41]
Sugarcane bagasse	24.70	[42]
Cashew nut shell	14.29	[43]
Coffee grounds	15.65	[44]
Calcium Alginate Beads	32.94	[45]
Activated carbon (Filtrasorb 400)	307.50	[46]
Nanometre scale HAP (Needle shape 20 to 30 nm)	142.86	[11]
Nanometre scale HAP (Spherical particles 30 nm)	123.45	Present Study

In addition, a comparative evaluation of the Cd^{2+} adsorption efficiency of the nanometre scale HAP absorber used in the present study and several other materials reported in the literature is made via Table 3. Inspection of Table 3 reveals the HAP absorber used in this study possesses a higher adsorption capacity to many other materials reported in the [11] listed in the table. But only activated carbon base materials such as Filtrasorb 400 have higher adsorption capacities [46].

3.7. The Effect of Temperature

An isothermal study was also carried out to investigate the effect of temperature on cadmium adsorption of HAP absorber. The five isotherms used were 283, 293, 303, 313 and 323 K, while the initial Cd^{2+} ion concentration (100 mg/L), contact time (300 min) and adsorbent dose (1 g/L) were kept constant during the study. The study revealed cadmium adsorption capacity steadily increased with increasing temperature [see Figure 4 (d)] and indicated the adsorption process was endothermic in nature.

To investigate the thermodynamics of the adsorption process, parameters such as free energy change (ΔG^0), enthalpy change (ΔH^0) and entropy change (ΔS^0) were calculated using the following equations:

$$\Delta G^0 = -RT\ln K \tag{8}$$

$$\Delta G^0 = \Delta H^0 - T\Delta S^0 \tag{9}$$

For the purpose of producing a linear graphical representation, equations (8) and (9) were combined and rearranged to give Van't Hoff equation:

$$\ln K = \frac{\Delta S^0}{R} - \frac{\Delta H^0}{RT} \tag{10}$$

where R is the universal gas constant (8.314 J mol^{-1} K^{-1}), T is the temperature in Kelvin and K is the thermodynamic equilibrium constant in units of L/g and is generally expressed by:

$$K = \frac{q_e}{C_e} \tag{11}$$

In order to ensure that K in equation (11) is dimensionless we have adopted the method suggested by Milonjic in which the equilibrium constant K is replaced with a new dimensionless equilibrium constant K_d [39]:

$$K_d = \frac{\rho q_e}{c_e} \tag{12}$$

where ρ is the density of water (~1000 g/L) and is assumed to remain constant over the entire temperature range studied and contains only a small absorber dose.

Values of K_d were calculated from the equilibrium concentrations over the temperature range. The values were found to increase with increasing temperature and revealed adsorption was endothermic in nature. The calculated changes in Gibbs free energy ΔG^0 were plotted against temperature T (K) and from the graph values of ΔH^0 (slope) and ΔS^0 (intercept) were determined (Graphs not shown). However, the thermodynamic parameters derived from this analysis are presented in Table 4. Inspection of Table 4 reveals that each of the ΔG^0 values are negative for each isotherm. The result indicates cadmium adsorption is spontaneous in nature and the adsorption process is enhanced with increasing temperature. The positive value of ΔH^0 (6872.12 J mol^{-1}) indicates the endothermic nature of the adsorption process and the positive value of ΔS^0 (90.06 J mol^{-1} K^{-1}) indicates the affinity of the nanometre scale HAP absorber for Cd^{2+} ions. The positive values of both ΔH^0 and ΔS^0 are also responsible for making the reaction spontaneous, irreversible in nature and also suggest that there were some structural changes to the absorber. Throughout Cd^{2+} ion removal from solution two distinct stages were clearly seen.

Table 4. Thermodynamic parameters for Cd^{2+} adsorption onto nanometre scale hydroxyapatite

Temperature (K)	K_d	ΔG^o (J/mol)	ΔH^o (J/mol)	ΔS^o (J/mol K)
283	2773.58	-18653.24	6872.12	90.06
293	3000.00	-19503.53		
303	3255.32	-20374.94		
313	3545.45	-21269.55		
323	4000.00	-22273.02		

During the first stage P-OH surface groups located on the absorber surface promoted surface complex's to take place. The FT-IR spectroscopy analysis presented in Figure 3 confirms this stage. Since the 600 and 631cm^{-1} peak intensities normally associated with P–OH groups were significantly reduced after Cd^{2+} ion adsorption had taken place. The reduction in peak intensity reflects the significant reduction in the number of free sites available for attachment to take place. During the second stage significant numbers of Cd^{2+} ions were substituted for Ca^{2+} ions in the HAP crystal lattice. The presence of cadmium in both the XRD and EDS analysis confirms the ion-exchange mechanism. The adsorption process can be described by the following equation:

$$Ca_{10}(PO_4)_6(OH)_2 + xCd^{2+} \rightarrow Ca_{10-x}Cd_x(PO_4)_6(OH)_2 + xCa^{2+} \tag{13}$$

It is during the second stage when there is partial dissolution of calcium from the HAP lattice that results in a apatite precipitation described by Ca_{10-x} Cd_x $(PO_4)_6(OH)_2$ and Ca^{2+} ions.

4. Conclusions

The present study has shown a HAP powder synthesized via a combined ultrasound and microwave based technique has resulted in the development of a highly crystalline structure with a spherical mean particle size of 30 nm. The prepared nanometre scale HAP powder was found to be an effective adsorbent for the removal of Cd^{2+} cations from aqueous solutions. The sorption performance was found to be a function of initial Cd^{2+} concentration, temperature and solution pH. Furthermore, Cd^{2+} removal was found to improve with increases in these parameters for specific contact times. The study also confirmed the sorption process was endothermic in nature and Cd^{2+} sorption increased with temperature. Kinetic studies revealed the sorption process closely followed pseudo-second order kinetics. During sorption, the initial uptake rate of Cd^{2+} was high, but this was followed by a much lower uptake rate. The ion-exchange mechanism ($Cd^{2+} \rightarrow Ca^{2+}$) was clearly identified as the major participant in the sorption process. The results of both XRD and EDS analysis confirmed ion-exchange was a major removal mechanism and sorption was heavily influenced by intra-particle diffusion. Isotherm studies indicated the Freundlich isotherm modelled experimental data better than the Langmuir isotherm. However, the Langmuir isotherm was used to determine maximum adsorption capacity of the HAP absorber and was found to be 123.45 mg/g. All calculated thermodynamic parameters (ΔG^o, ΔH^o and ΔS^o) clearly indicate sorption was thermodynamically favourable, endothermic and spontaneous in nature.

ACKNOWLEDGEMENTS

Ms. Sridevi Brundavanam would like to acknowledge Murdoch University for providing a PhD Scholarship to undertake the cadmium adsorption studies as part of her PhD project.

REFERENCES

[1] Wongsasuluk, P., Chotpantarat, S., Siriwong, W., Robson, M., 2012, Heavy metal contamination and health risk assessment in drinking water from shallow groundwater wells in an agricultural area in Ubon Ratchathani province, Thailand.

Environ Geochem. Health, 36, 169-182.

[2] Jarup, L., 2003, Hazards of heavy metal contamination, British Medical Bulletin, 68 (1), 167-182.

[3] Hartwig, A., 2013, Cadmium and cancer, Met. Ion. Life. Sci., 11, 491-507.

[4] Mulligan, C.N., Yong, R.N., Gibbs, B.F., 2001, Remediation technologies for metal-contaminated soils and groundwater: an evaluation, Eng. Geol., 60, 193–207.

[5] Ramos, R.L., Mendez, J.R.R., Baron, J.M., Rubio, L.F., Coronado, R.M.G., 1997, Adsorption of cadmium (II) from aqueous solution onto activated carbon, Water Sci. Technol., 5 (7), 205-211.

[6] Zhu, R., Yu, R., Yao, J., Mao, D., Xing, C., Wang, D., 2008, Removal of Cd^{2+} from aqueous solutions by hydroxyapatite, Catalysis Today, 139, 94–99.

[7] Kaji, M., 2012, Role of experts and public participation in pollution control: the case of Itai-itai disease in Japan, Ethics Sci. Environ Polit., 12, 99-111.

[8] Barakat, M.A., 2011, New trends in removing heavy metals from industrial wastewater. Arabian Journal of Chemistry, 4 (4), 361-377.

[9] Al-Enezi, G., Hamoda, M.F., Fawzi, N., 2004, Ion exchange of heavy metals from wastewater sludges, J. Environ Sci. Health A Tox. Hazard Subst. Environ. Eng., 39 (2), 455-464.

[10] Nhapi, I., Banadda, N., Murenzi, R., Sekomo, C.B., Wali, U.G., 2011, Removal of heavy metals from industrial wastewater using rice husks, The open Environmental Engineering Journal, 4, 170-180.

[11] Mobasherpour, I., Salahi, E., Pazouki, M., 2011, Removal of divalent cadmium cations by means of synthetic nano-crystallite hydroxyapatite, Desalination, 266, 142–148.

[12] Mohan, D., and Singh, K.P., 2002, Single and multi-component adsorption of cadmium and zinc activated carbon derived from bagasse–an agricultural waste, Water Res., 26, 2304-2318.

[13] Reichert, J., and Binner, J.G.P., 1996, An evaluation of hydroxyapatite-based filters for removal of heavy metal ions from aqueous solutions, Journal of Materials Science, 31, 1231–1241.

[14] Del Rio, J.G., Sanchez, P., Morando, P.J., Cicerone, D.S., 2006, Retention of Cd, Zn, and Co on hydroxyapatite filters, Chemosphere, 64, 1015–1020.

[15] Poinern, G.E.J., Brundavanam, R., Le, X., Djordjevic, S., Prokic, M., Fawcett, D., 2011, Thermal and ultrasonic influence in the formation of nanometre scale hydroxyapatite bio-ceramic, International Journal of Nanomedicine, 6, 2083-2095.

[16] Dorozhkin, S.V., 2009, Nanodimensional and nanocrystalline apatites and other calcium orthophosphates in biomedical engineering, biology and medicine. Materials, 2, 1975-2045.

[17] Poinern, G.E.J., Brundavanam, R., Le, X., Nicholls, P.K., Cake, M.A., Fawcett, D., 2014, The synthesis, characterisation and in vivo study of a bioceramic for potential tissue regeneration applications, Scientific Reports, 4, 6235, 1-9.

[18] Tanaka, H., Futaoka, M., Hino, R., Kandori, K., Ishikawa, T., 2005, Structure of synthetic calcium hydroxyapatite particles modified with pyrophosphoric acid, J. Colloid Interface. Sci. 283 (2), 609-612.

[19] Monteil Rivera, F., and Fedoroff, M., Sorption of inorganic species on apatite's from aqueous solutions: In Encyclopaedia of surface and colloid Science. Marcel Dekker. Inc, New York, 2002.

[20] Phillips, M.J., Darr, J.A., Luklinska, Z.B., Rehman, I., 2003, Synthesis and characterization of nano-biomaterials with potential osteological applications, J. Mater. Sci. Mater. Med. 14, 875-882.

[21] Chaudhry, A.A., Haque, S., Kellici, S., Boldrin, P., Rehman, I., Khalid, F.A., Darr, J.A., 2006, Instant nano-hydroxyapatite: a continuous and rapid hydrothermal synthesis, Chem. Commun., 2286-2288.

[22] Kuriakose, T.A., Kalkura, S.N., Palanichamy, M., Arivuoli, D., Dierks, K., Bocelli, G., Betzel, C., 2004, Synthesis of stoichiometric nano-crystalline hydroxyapatite by ethanol-based sol-gel technique at low temperature, J. Cryst. Growth, 263, 517-523.

[23] Majumdar, S., Chakraborty, S., Devi, P.S., Sen, A., 2008, Room temperature synthesis of nanocrystalline SnO through sonochemical route, Mater. Lett., 62, 1249-1251.

[24] Poinern, G.E.J., Brundavanam, R., Mondinos, N., Jiang, Z.T., 2009, Synthesis and characterization of nanohydroxyapatite using an ultrasound assisted method, Ultrasonics Sonochemistry, 16, 469-474.

[25] McNamara, W.B., Didenko, Y.T., Suslick, K.S., 1999, Sonoluminescence temperatures during multi-bubble cavitation, Nature, 401, 772–775.

[26] Cao, L.Y., Zhang, C., Huang, J.F., 2005, Influence of temperature, $[Ca^{2+}]$, Ca/P ratio and ultrasonic power on the crystallinity and morphology of hydroxyapatite nanoparticles prepared with a novel ultrasonic precipitation method, Mater. Lett., 59, 1902-1906.

[27] Meejoo, S., Maneeprakom, W., Winotai, P., 2006, Phase and thermal stability of nanocrystalline hydroxyapatite prepared via microwave heating, Thermochim. Acta., 447, 115-120.

[28] Poinern, G. E. J., Brundavanam, R., Le, X., Fawcett, D., 2012, The mechanical properties of a porous ceramic derived from a 30 nm sized particles based powder of hydroxyapatite for potential hard tissue engineering applications. Am. J. Biomed. Eng., 2, 278-286.

[29] Danilchenko, S.N., Kukharenko, O.G., Moseke, C., Protsenko, I.Y., Sukhodub, L.F., Sulkio-Cleff, B., 2002, Determination of the bone mineral crystallite size and lattice strain from diffraction line broadening, Cryst. Res. Technol., 37 (11), 1234-1240.

[30] Klug, H.P., and Alexander, L.E., 1974, X-ray diffraction procedures for poly-crystallite and amorphous materials. 2nd Ed., Wiley, New York.

[31] Barrett, C.S., Cohen, J.B., Faber, J., Jenkins, J.R., Leyden, D.E., Russ, J.C., Predecki, P.K., 1986, Advances in X-ray analysis, Vol. 29, Plenum Press, New York.

[32] Lee, C.K., Kim, H.S., Kwon, J.H., 2005, The removal of heavy metals using hydroxyapatite, Environ. Eng. Res., 10 (5),

205-212.

[33] Evisa, Z., Yilmazb, B., Ustac, M., Aktugc, A.L., 2013, X-ray investigation of sintered cadmium doped hydroxyapatites, Ceramics International, 39, 2359–2363.

[34] Panda, R.N., Hsieh, M.F., Chung, R.J., Chin, T.S., 2003, FTIR, XRD, SEM and solid state NMR investigations of carbonate-containing hydroyapatite nano-particles synthesised by hydroxide-gel technique, J. Physics and Chemistry of Solids, 64 (2), 193-199.

[35] Wang, Y., Zhang, S., Wei, K., Zhao, N., Chen, J., Wang, X., 2006, Hydrothermal synthesis of hydroxyapatite nanopowders using cationic surfactant as a template. Mater Lett., 60 (12),1484-1487.

[36] Lagergren, S., 1898, Zur theorie der sogenannten adsorption gelöster stoffe, Kungliga Svenska Vetenskapsakademiens Handlingar, 24, 1-39.

[37] McKay, G., Ho, Y.S., 1999, Pseudo-second order model for sorption processes, Process Biochem., 34, 451-465.

[38] Weber, W.J., and Morris, J.C., 1963, Kinetics of adsorption on carbon from solution, J. Sanit. Engng. Div. Am. Soc. Civ. Engrs, 89, 31-60.

[39] Milonjic, S.K., 2007, A consideration of the correct calculation of thermodynamic parameters of adsorption, J. Serb. Chem. Soc., 72, 1363–1367.

[40] Ajmal, M., Rao, R.A., Anwar, S., Ahmad, J., Ahmad, R., 2003, Adsorption studies on rice husk: removal and recovery of Cd (II) from wastewater, Bioresource Technol., 86, 147–149.

[41] Al-Anber, Z.A., and Matouq, M.A.D., 2008, Batch adsorption of cadmium ions from aqueous solution by means of olive cake, J. Hazard Mater., 151 (1), 194–201.

[42] Krishnan, K.A., Anirudhan, T.S., 2003, Removal of cadmium (II) from aqueous solutions by steam activated sulphurised carbon prepared from sugar-cane bagasse pith: kinetics and equilibrium studies, Water SA, 29, 147–156.

[43] Tangjuank, S., Insuk, N., Tontrakoon, J., Udeye, V., 2009, Adsorption of Lead (II) and Cadmium (II) ions from aqueous solutions by adsorption on activated carbon prepared from cashew nut shells, World Acad. Sci. Eng. Technol., 52, 110–116.

[44] Azouaoua, N., Sadaouia, Z., Djaafri, A., Mokaddema, H., 2010, Adsorption of cadmium from aqueous solution onto untreated coffee grounds: equilibrium, kinetics and thermodynamics, J Hazard Mater., 184 (1–3), 126–134.

[45] Alfaro-Cuevas-Villanueva, R, Hidalgo-Vázquez, A.R., Cortés-Penagos, C., Cortés-Martínez, R., 2014, Thermodynamic, Kinetic, and Equilibrium Parameters for the Removal of Lead and Cadmium from Aqueous Solutions with Calcium Alginate Beads. Scientific World Journal, Volume 2014: Article ID 647512, 9 pages.

[46] Kapoor, A., Viraraghavan, T., Cullimore, D.R., 1999, Removal of heavy metals using the fungus Aspergillus niger, Bioresource Technol., 70 (1), 95-104.